

**Nonperturbative effects of deep strong light-matter interaction in a mesoscopic cavity-QED system**A. Kudlis,<sup>1</sup> D. Novokreschenov,<sup>2</sup> I. Iorsh,<sup>1,2,\*</sup> and I. V. Tokatly<sup>3,4,5,2</sup><sup>1</sup>*Abrikosov Center for Theoretical Physics, MIPT, Dolgoprudnyi, Moscow Region 141701, Russia*<sup>2</sup>*Faculty of Physics, ITMO University, St. Petersburg 197101, Russia*<sup>3</sup>*Nano-Bio Spectroscopy Group and European Theoretical Spectroscopy Facility (ETSF),**Departamento de Polímeros y Materiales Avanzados: Física,**Química y Tecnología, Universidad del País Vasco, Avenida Tolosa 72, E-20018 San Sebastián, Spain*<sup>4</sup>*IKERBASQUE, Basque Foundation for Science, 48009 Bilbao, Spain*<sup>5</sup>*Donostia International Physics Center (DIPC), E-20018 Donostia-San Sebastián, Spain*

(Received 11 April 2023; accepted 23 October 2023; published 13 November 2023)

We consider a system comprising two groups of quantum dimers placed in a common electromagnetic cavity and controlled by selectively applying a static external potential to one of the groups. We show that in the regime of deep strong coupling to vacuum electromagnetic fluctuations, the emergent photon-assisted interaction between the dimers, leads to a strongly nonlinear quantized cross-polarization response of the first, unbiased group of dimers to the potential applied to the second group. The total polarization shows a series of almost ideal steps whose number and position depends on the parity of the numbers of dimers in the groups. This nonperturbative effect is a distinctive feature of mesoscopic systems comprising a finite number of dimers and disappears in the thermodynamic limit which is commonly used in the description of the generalized Dicke models.

DOI: [10.1103/PhysRevA.108.L051701](https://doi.org/10.1103/PhysRevA.108.L051701)

Polaritonic chemistry [1,2], a novel rapidly developing interdisciplinary field, explores methods to modify chemical properties of materials by placing them inside optical microcavities. Of particular interest is the regime of strong light-matter coupling when the characteristic energy of the light-matter interaction exceeds the decay rates of the individual excitations leading to the emergence of the hybrid light-matter quasiparticles, polaritons. Due to the photonic component, polaritons preserve spatial coherence at large distances of the order of the resonant cavity wavelength, which as has been shown both theoretically [3] and experimentally [4] leads to the substantial modification of energy transfer and more generally chemical kinetics in cavity-embedded materials. Moreover, for stronger light-matter interaction, when the characteristic energy of light-matter coupling becomes comparable to the excitation energy, the system enters the so-called ultrastrong coupling regime [5] characterized by the substantial modification of the ground state of the system by vacuum fluctuations of cavity electromagnetic field. Ultrastrong coupling was predicted to induce various cavity-mediated phase transitions such as superconductivity [6–10], ferroelectric phase transitions [11], and topological phase transitions [12,13], as well as substantial modification of the chemical reactions inside the cavity [14].

Theoretical description of the ultrastrong coupling between light and matter usually focuses at the two limiting cases. First, one can consider a very small number of two-level systems coupled to the cavity modes of the system. In the limit of a single cavity mode and one two-level system this

reduces to the celebrated Rabi model, for which an analytical solution has been found relatively recently [15]. In the opposing limit of large number  $N$  of two-level systems, one can exploit the transition to the thermodynamic limit  $N \rightarrow \infty$ . It has been shown that in this limit one may resort to the random phase approximation in the leading order with respect to  $1/N$  [16–18].

The intermediate case, when the number  $N$  is finite but not asymptotically large, corresponding to the mesoscopic regime, is largely *terra incognita* so far. In this intermediate case, there are not many methods except for the computationally demanding exact diagonalization of the full light-matter Hamiltonian. While recently new approaches based on the quantum electrodynamics density functional theory developed [19–24], their applicability to generic systems in the ultrastrong coupling regime is still a subject of active research.

In this Letter we explore this intermediate regime of finite number of two-level systems in a cavity and demonstrate the emergence of the nonperturbative effects which cannot be described within the RPA. Specifically, we consider a system schematically depicted in Fig. 1:  $N = N_1 + N_2$  dimers are placed in a single-mode cavity. Only  $N_2$  dimers are subject to the external static potential  $v_{\text{ext}}$ , polarizing the dimers. It is assumed that dimers do not interact directly and are coupled only via the interaction with a cavity electromagnetic mode.

The Hamiltonian of the system reads

$$\hat{H} = -T \sum_{i=1}^N \hat{\sigma}_{i,x} + v_{\text{ext}} \sum_{i=N_1+1}^N \hat{\sigma}_{i,z} + \frac{\hat{p}^2}{2} + \frac{\lambda^2}{2} \left( \frac{\omega \hat{q}}{\lambda} - \sum_{i=1}^N \hat{\sigma}_{i,z} \right)^2. \quad (1)$$

\*i.iorsh@metalab.ifmo.ru

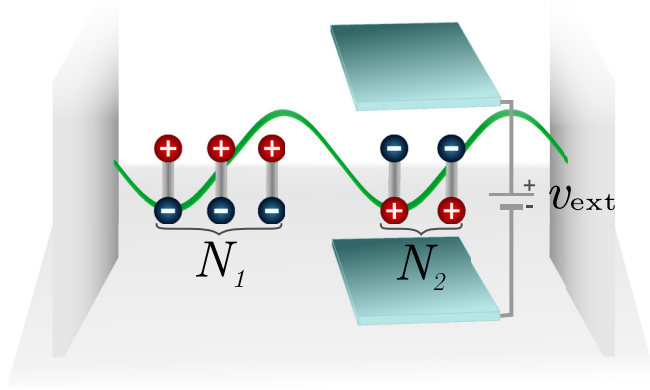


FIG. 1. Schematic representation of the setup: two groups of dimers in the cavity with a polarizing potential applied to one of the groups. Interaction between dimers is allowed only via photonic mode. In the shown configuration  $N_1 = 3$  and  $N_2 = 2$ , antiferroelectric ordering is observed.

The first term describes the tunneling of the electrons between two states in each dimer with  $T$  being intradimer hopping amplitude. An experimental realization which corresponds to this model is an ensemble of the diatomic molecules or double quantum dots. The tunneling term thus describes electron hopping between two atoms or two quantum dots. We neglect direct coupling between dimers, which is justified since the tunneling coefficient decays exponentially with the distance. The second term describes the static gating of the one group of the dimers. Indeed, when a static electric field is applied along the dimer direction, the energies of the two dimer sites are split. The last two terms correspond to the energy  $1/8\pi \int (\hat{\mathbf{B}}^2 + \hat{\mathbf{E}}^2) d\mathbf{r}$  of the transverse cavity mode. The magnetic field  $\hat{\mathbf{B}} = \sqrt{4\pi} \hat{\mathbf{p}}$  is proportional to the photon canonical momenta  $\hat{\mathbf{p}}$ . The electric field  $\hat{\mathbf{E}} = \sqrt{4\pi} (\omega \hat{q} - \lambda \hat{S}_z)$  is related to canonical coordinate  $\hat{q}$ , proportional to the electric displacement, and  $\lambda \sum_i \hat{\sigma}_{iz}$  is the total polarization of the system of dimers with  $\lambda$  being the effective light-matter interaction. In what follows we normalize the energy to the cavity photon energy  $\omega$ . It should be noted the Hamiltonian (1) belongs to a class of so-called generalized Dicke models which have been studied recently [25–32]. Specifically, it has been shown that the structure of the ground state [28] and thermodynamic properties [26] of such systems can substantially deviate from the predictions of the conventional Dicke model. A common feature of these models are the emergent long-range interactions between the two-level systems facilitated by the exchange of the cavity photon. There was also a certain ambiguity related to the question whether these systems may support a so-called Dicke superradiant phase transition with the emergence of polarization in the ground state. It is, however, now acknowledged that in the gauge-invariant formulations of these models, this phase transition is absent in the case of spatially uniform cavity mode profiles [33–35]. Specifically, Hamiltonian (1) is gauge equivalent to a collection of dimers with intradimer hoppings dressed with an electromagnetic vector potential via Peierls substitution.

We are interested in the dependence of polarization (which is given by operator  $\sigma_z$  for each dimer) for the first group of

dimers on the external potential  $v_{\text{ext}}$  applied to the second group. We used the exact diagonalization to find the ground state of the system. In what follows we will use the operators of the polarization of the groups of the dimers:  $\hat{\mathbf{S}}_{(1,2)} = \sum_{i=1}^{N_{(1,2)}} \hat{\sigma}^{(1,2),i}$  and the total polarization  $\hat{\mathbf{S}} = \hat{\mathbf{S}}_1 + \hat{\mathbf{S}}_2$ .

Figure 2 shows two examples of the dependence on  $v_{\text{ext}}$  of the average polarization for each group of dimers  $d_{(1,2)} = 1/N_{(1,2)} \sum_{i=1}^{N_{(1,2)}} \langle \sigma_z^{(1,2),i} \rangle$  and of the total polarization  $P = \langle S_z \rangle$ . Specifically, we present two cases: ( $N_1 = 1, N_2 = 2$ ) and ( $N_1 = 2, N_2 = 2$ ). The main common features of the presented dependencies are (i) a strongly nonmonotonic discontinuous average polarization of first group  $d_1(v_{\text{ext}})$  and (ii) a sharp, steplike total polarization  $P(v_{\text{ext}})$ . We also observe remarkable differences in the behavior for these two cases, both at large and at small  $v_{\text{ext}}$ . First, at large  $|v_{\text{ext}}|$  the polarizations of the two groups of dimers have opposite signs for  $N_1 = 1$  and the same sign for  $N_1 = 2$ . Moreover, at  $v_{\text{ext}} \approx 0$  the polarization is almost constant for  $N_1 = 2$  and has a steep step for  $N_1 = 1$ . The plots for other combinations of ( $N_1, N_2$ ) can be found in the Supplemental Material [36].

Importantly, the observed peculiar quantized response emerges only in the deep strong coupling regime when the dimensionless light-matter coupling strength  $\lambda^2/\omega \geq 1$ . In this regime, one can neglect the kinetic energy of the harmonic oscillator in Hamiltonian (1) and treat  $q$  as a classical variable, which can be viewed as a cavity Born-Oppenheimer approximation (BOA) [37]. In this approximation, the Hamiltonian reduces to a square matrix of dimension  $(N_1 + 1) \times (N_2 + 1)$ , and we can find its ground state by finding the lowest eigenvalue  $E(q)$  at each  $q$  (the BO surface) and then identifying its global minimum. As can be seen in Fig. 2 the polarization found in this approximation (shown with blue dotted lines) reproduces all main features of the exact diagonalization (shown with dashed blue lines).

We then make yet another approximation: we first switch off the intradimer hopping  $T = 0$  and then switch it on adiabatically. In the limit  $T = 0$  the Hamiltonian can be diagonalized exactly. The eigenstates are just the direct products of the eigenstates of  $S_{1,z}, S_{2,z}$ ,  $|m_1, m_2\rangle = |m_1\rangle \otimes |m_2\rangle$ . For each group of dimers there are  $N_i + 1$  distinct eigenvalues values  $m_i = -N_i, -N_i + 2, \dots, N_i - 2, N_i$ . The ground-state energy is then given by

$$E_{T=0} = \min_q \left[ v_{\text{ext}} m_2 + \frac{\lambda^2}{2} \left( \frac{\omega q}{\lambda} - m_1 - m_2 \right)^2 \right]. \quad (2)$$

In this case  $E_{T=0}$  has local minima at points  $\omega q/\lambda = m_1 + m_2 = -N, \dots, N$ , and in total there are  $N + 1$  minima. For even  $N$  (odd number of minima), all minima are located at even integer values of  $\omega q/\lambda$  ( $\dots, -4, -2, 0, 2, 4, \dots$ ), and there is a distinguished central minimum with  $m = 0$ . For odd  $N$  (even number of minima) they are also at integer points ( $\dots, -3, -1, 1, 3, \dots$ ), but the integers are odd and the minimum at  $q = 0$  is absent. At  $T = 0$  and  $v_{\text{ext}} = 0$  all  $N + 1$  minima in the BO surface are degenerate in energy. At finite  $v_{\text{ext}}$  the number of degenerate valleys reduces to  $N_1 + 1$ , while the energies of the remaining  $N_2$  minima acquire a linear dependence on  $m_2$ . This multivalley structure of the BO surface controlled by  $v_{\text{ext}}$  is the root of the steplike behavior of the total polarization  $P$ .

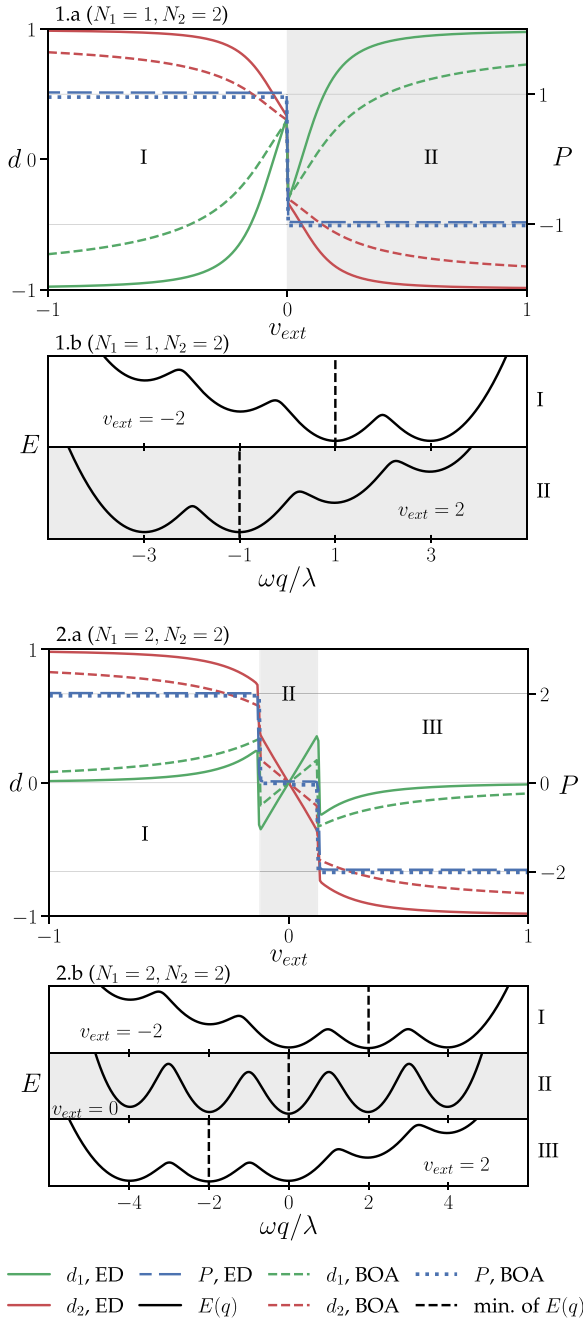


FIG. 2. Dependencies of  $d_1$ ,  $d_2$ , and  $P$  (upper panel in each figure) on the external field  $v_{\text{ext}}$  applied to the second group of dimers, and semiclassical Born-Oppenheimer (BO) ground-state energies as functions of the rescaled photon coordinate  $\omega q/\lambda$  in different ranges of  $v_{\text{ext}}$  (lower panels in each figure). The upper figure corresponds to the combination  $N_1 = 1$  and  $N_2 = 2$ . For the lower figure,  $N_1 = 2$  and  $N_2 = 2$ . In both cases the system parameters are  $\lambda = 3$ ,  $\omega = 1$ ,  $T = 1$ . BOA and ED denote Born-Oppenheimer approximation and exact diagonalization, respectively.

The degeneracy of different minima is lifted by turning on the intradimer hopping  $T$ , which introduces coupling between states corresponding to different eigenstates of the  $S_z$  operator at the same  $q$ . The operator  $TS_x$  couples the states with  $S_z$  projections which differ by  $\pm 2$ . Therefore the correction to the energy starts from the second order and generically

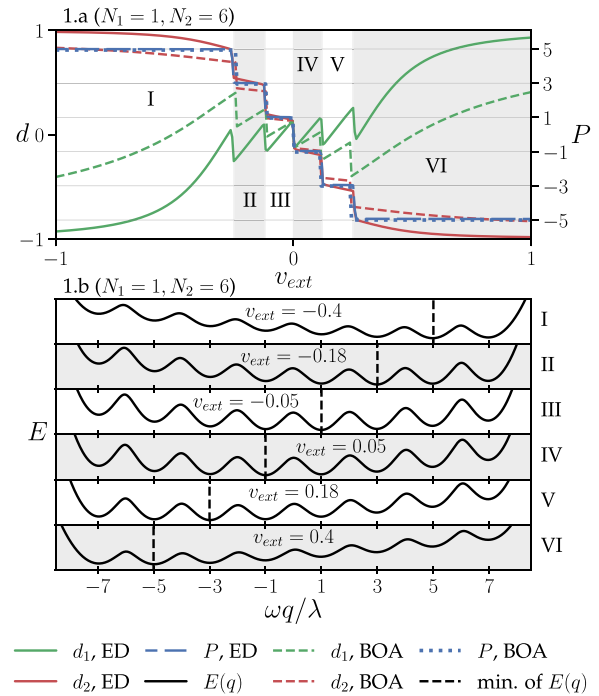


FIG. 3. Dependencies of  $d_1$ ,  $d_2$ , and  $P$  on  $v_{\text{ext}}$  applied to the second group of dimers (upper panel), and the BO energies in different ranges of  $v_{\text{ext}}$  as functions of the photon coordinate  $q$  (lower panels). The figure corresponds to  $N_1 = 1$ ,  $N_2 = 6$ . System parameters are  $\lambda = 3$ ,  $\omega = 1$ ,  $T = 1$ .

lowers the ground-state energy. Moreover, the correction due to the coupling between states with projections different by  $2n$  (where  $n$  is a positive integer) will be proportional to  $(T/\lambda^2)^n$ . Apparently for  $v_{\text{ext}} = 0$ , the lowest energy corresponds to minima with smallest  $|q|$  ( $q = 0$  for even  $N$  and  $\omega q/\lambda = \pm 1$  for odd  $N$ ). Indeed, for even  $N$ , the central minimum at  $q = 0$  acquires a downward shift that is by an amount  $\sim (T/\lambda^2)^{\frac{N}{2}}$  larger compared to the shift of the neighboring minima at  $\omega q/\lambda = \pm 2$ . For odd  $N$ , the two degenerate central minima at  $\omega q/\lambda = \pm 1$  are redshifted with respect to the closest minima at  $\omega q/\lambda = \pm 3$  by a term  $\sim (T/\lambda^2)^{\frac{N-1}{2}}$ . This simple analysis is confirmed by computing the BO energies numerically; see lower panels in Figs. 2 and 3.

In the case of odd  $N$ , a weak external potential  $v_{\text{ext}}$  lifts the degeneracy between the  $\omega q/\lambda = \pm 1$  states, and the system falls to one of these minima depending on the sign of  $v_{\text{ext}}$ . This results in the steplike behavior of polarization at  $v_{\text{ext}} \approx 0$  shown in Fig. 2 for  $N = 3$ , and in Fig. 3 for  $N = 7$ . For even  $N$  there is a single minimum at  $q = 0$ , and the system remains in this minimum for small  $v_{\text{ext}}$ , as we can see in Fig. 2 for  $N = 4$ . In general, a finite  $v_{\text{ext}}$  favors the extreme values of  $m_2 = \pm N_2$  in order to minimize term  $v_{\text{ext}} m_2$ . In the limit  $T = 0$  there are thus  $N_1 + 1$  degenerate minima corresponding to  $m_2 = -N_2$  (for positive  $v_{\text{ext}}$ ) and for  $\omega q/\lambda = m_1 + N_2$  and  $N_2$  states with values of  $m_2$  from  $-N_2 + 2$  to  $N_2$ . Nonzero  $T$  couples states with different  $S_z$  and lifts the degeneracy. However, in the presence of  $v_{\text{ext}}$  the global minimum does not always correspond to the state with smallest  $S_z$ , because there we find the energy asymmetry for the states with  $S_z$  differing by  $\pm 2$ . As a result for small  $v_{\text{ext}}$ , the global energy minimum

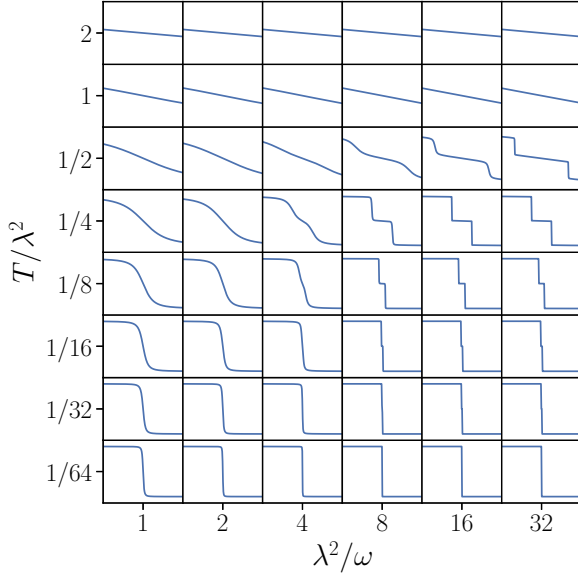


FIG. 4. Polarization  $P$  as a function of  $v_{\text{ext}}$  for different values of  $T/\lambda^2$  and  $\lambda^2/\omega$ . Each cell shows  $P$  within limits  $[-2.5; 2.5]$  when  $v_{\text{ext}}$  changes in the range  $[-2; 2]$ . The system corresponds to  $N_1 = 2$  and  $N_2 = 2$  at  $\lambda = 3$ .

still corresponds to the valley with the minimal  $S_z$ , but as  $v_{\text{ext}}$  becomes comparable to  $T^2/\lambda^2$  the system switches to the state with another value of  $S_z$ . This results in the stepwise dependence of the polarization on  $v_{\text{ext}}$  with the width of the steps proportional to  $T^2/\lambda^2$ . The total number of steps  $N_s$  obeys a simple formula

$$N_s = \begin{cases} N_2 - 1, & \text{if } N_1 \text{ is odd} \\ N_2, & \text{if } N_1 \text{ is even} \end{cases}. \quad (3)$$

The validity of this formula is clearly demonstrated by Figs. 2 and 3. We provide a chart of characteristic plots for different  $N$  in Fig. 3 of the Supplemental Material [36].

The quantum nature of electromagnetic field is responsible for transitions between the steps because they occur via tunneling between the corresponding valleys of the BO surface. To account for this, we replace the variable  $q$  by a coherent state  $|q\rangle$  of the harmonic oscillator, such that  $\langle q|\hat{q}|q\rangle = q$ . The wave function can then be written as a linear combination of the coherent states corresponding to different local minima of the BO surface. The tunneling probability between the minima at different  $q_i$  is proportional to the overlap of the corresponding coherent states  $\langle q_i|q_j\rangle \sim e^{-(q_i-q_j)^2} \sim e^{-\lambda^2/\omega}$ . Thus, the parameter  $\lambda^2/\omega$  controls the coupling between the valley with different  $q$ , and  $e^{-\lambda^2/\omega}$  determines the width of the steep transition between the states with corresponding  $S_z$ . To illustrate the dependence of the shape of the steps on  $T/\lambda^2$  and  $\lambda^2/\omega$ , in Fig. 4 we plot a collection of the step shapes for different values of these two parameters.

It should be emphasized that the observed steplike behavior disappears in the thermodynamic limit. We demonstrate it explicitly using a numerical calculation, the results of which are shown in Fig. 3 in the Supplemental Material [36]. This limit corresponds to  $N \rightarrow \infty$  and the scaling of the light-matter

$$\begin{aligned} \text{RPA:} & \quad \text{Diagram} = c_1 + a_1 v_{\text{ext},1}^2 + b_1 v_{\text{ext},2}^2 + \dots \\ \text{NONRPA:} & \quad \text{Diagram} = c_2 + a_2 v_{\text{ext},1} v_{\text{ext},2} + \dots \end{aligned}$$

FIG. 5. Difference in behavior between the two types of diagrams. It can be seen that the cross-susceptibility ( $\chi_{12}$ ), which simply is equal to the cross-derivative from diagrams above, in the RPA case is zero if the field on one of the dimers is always zero. Explicit expressions for  $a_1, c_1, b_1, c_2, a_2$  are presented in the Supplemental Material [36].

interaction as  $\lambda \rightarrow \lambda/\sqrt{N}$  as it is inversely proportional to the square root of the cavity mode volume. It is now anticipated that the thermodynamic limit of the Dicke and related models can be analyzed within the  $1/N$  expansion [16–18], and the leading order correction is given by the RPA-like bubble diagrams. The second-order RPA energy diagram is shown in the upper panel of Fig. 5. The bubbles correspond to the dimer excitation propagator and wavy lines to the cavity photon propagators. Each bubble has a factor of  $N_{1,2}$ , depending on the group of dimers, and each vertex carries a factor of  $\lambda/\sqrt{N}$ . Let us apply the external potentials  $v_{\text{ext},1}$  and  $v_{\text{ext},2}$  to the first and the second group of dimers, respectively. The differential cross-polarizability of the first group is given by  $\chi_{12} = \partial^2 E_0 / (\partial v_{\text{ext},1} \partial v_{\text{ext},2})|_{v_{\text{ext},1}=0}$ . The energy corrections can be expanded with respect to small  $v_{\text{ext}}$  and calculated explicitly. The result shows that for the RPA-like diagrams there are no terms in the energy proportional to  $v_{\text{ext},1} v_{\text{ext},2}$ , and thus the cross-polarizability is identically zero. The cross-terms appear in the next order of  $1/N$  expansion for the diagram shown in the lower panel of Fig. 5. Thus, the magnitude of the cross-polarization scales as  $\lambda^6/N$  and vanishes in the thermodynamic limit. Therefore, the effective dimer-dimer interaction emerges only in the case of mesoscopic systems, with a finite number of dimers.

An experimental observation of the proposed effect could be realized in the system comprising two spatially separated groups of double quantum dots embedded in a single microwave cavity [38–40]. It should be noted that in a realistic system, the cavity photons will have a finite lifetime due to the finite cavity quality factor, which may lead to the electroluminescence in the considered system. While electroluminescence was previously predicted in the similar setups [41], a self-consistent description of the spectral and statistical properties of the emission would require an input-output formalism supplemented with a density matrix master equation tailored for the ultrastrong coupling regime [32].

To conclude, we have shown that mesoscopic systems in the ultrastrong coupling regime demonstrate the nonperturbative behavior, not captured neither by the weak coupling perturbation or by the  $1/N$  expansion conventionally used for the description of the Dicke-like Hamiltonians. Specifically, in the system comprising two group of dimers in a common cavity, we have revealed a quantized dependence of the cross-polarization and the total polarization on the external potential applied selectively to one of the groups. We give a

qualitative explanation of the discovered effect and explain why it occurs only for finite numbers of dimers and a deep strong light-matter coupling regime. These results open routes to exploring physics of deep strong light-matter coupling in mesoscopic systems.

I.V.T. acknowledges support from Grupos Consolidados UPV/EHU del Gobierno Vasco (Grant No. IT1453-22) and from Grant No. PID2020-112811GB-I00 funded by MCIN/AEI/10.13039/501100011033. I.I. acknowledges the support of “Basis” Foundation and “Priority 2030” Program.

- 
- [1] T. W. Ebbesen, Hybrid light-matter states in a molecular and material science perspective, *Acc. Chem. Res.* **49**, 2403 (2016).
- [2] R. F. Ribeiro, L. A. Martínez-Martínez, M. Du, J. Campos-Gonzalez-Angulo, and J. Yuen-Zhou, Polariton chemistry: Controlling molecular dynamics with optical cavities, *Chem. Sci.* **9**, 6325 (2018).
- [3] F. Herrera and F. C. Spano, Cavity-controlled chemistry in molecular ensembles, *Phys. Rev. Lett.* **116**, 238301 (2016).
- [4] X. Zhong, T. Chervy, L. Zhang, A. Thomas, J. George, C. Genet, J. A. Hutchison, and T. W. Ebbesen, Energy transfer between spatially separated entangled molecules, *Angew. Chem.* **129**, 9162 (2017).
- [5] A. F. Kockum, A. Miranowicz, S. D. Liberato, S. Savasta, and F. Nori, Ultrastrong coupling between light and matter, *Nat. Rev. Phys.* **1**, 19 (2019).
- [6] A. Thomas, E. Devaux, K. Nagarajan, T. Chervy, M. Seidel, D. Hagenmüller, S. Schütz, J. Schachenmayer, C. Genet, G. Pupillo *et al.*, Exploring superconductivity under strong coupling with the vacuum electromagnetic field, [arXiv:1911.01459](https://arxiv.org/abs/1911.01459).
- [7] J. B. Curtis, Z. M. Raines, A. A. Allocca, M. Hafezi, and V. M. Galitski, Cavity quantum Eliashberg enhancement of superconductivity, *Phys. Rev. Lett.* **122**, 167002 (2019).
- [8] M. A. Sentef, M. Ruggenthaler, and A. Rubio, Cavity quantum-electrodynamical polaritonically enhanced electron-phonon coupling and its influence on superconductivity, *Sci. Adv.* **4**, eaau6969 (2018).
- [9] F. Schlawin, A. Cavalleri, and D. Jaksch, Cavity-mediated electron-photon superconductivity, *Phys. Rev. Lett.* **122**, 133602 (2019).
- [10] J. Li and M. Eckstein, Manipulating intertwined orders in solids with quantum light, *Phys. Rev. Lett.* **125**, 217402 (2020).
- [11] Y. Ashida, A. İmamoğlu, J. Faist, D. Jaksch, A. Cavalleri, and E. Demler, Quantum electrodynamic control of matter: Cavity-enhanced ferroelectric phase transition, *Phys. Rev. X* **10**, 041027 (2020).
- [12] D. Guerci, P. Simon, and C. Mora, Superradiant phase transition in electronic systems and emergent topological phases, *Phys. Rev. Lett.* **125**, 257604 (2020).
- [13] X. Wang, E. Ronca, and M. A. Sentef, Cavity quantum electrodynamical Chern insulator: Towards light-induced quantized anomalous Hall effect in graphene, *Phys. Rev. B* **99**, 235156 (2019).
- [14] L. A. Martínez-Martínez, R. F. Ribeiro, J. Campos-González-Angulo, and J. Yuen-Zhou, Can ultrastrong coupling change ground-state chemical reactions? *ACS Photonics* **5**, 167 (2018).
- [15] D. Braak, Integrability of the Rabi model, *Phys. Rev. Lett.* **107**, 100401 (2011).
- [16] O. Dmytruk and M. Schiró, Gauge fixing for strongly correlated electrons coupled to quantum light, *Phys. Rev. B* **103**, 075131 (2021).
- [17] O. Dmytruk and M. Schiró, Controlling topological phases of matter with quantum light, *Commun. Phys.* **5**, 271 (2022).
- [18] K. Lenk, J. Li, P. Werner, and M. Eckstein, Collective theory for an interacting solid in a single-mode cavity, [arXiv:2205.05559](https://arxiv.org/abs/2205.05559).
- [19] I. V. Tokatly, Time-dependent density functional theory for many-electron systems interacting with cavity photons, *Phys. Rev. Lett.* **110**, 233001 (2013).
- [20] M. Ruggenthaler, J. Flick, C. Pellegrini, H. Appel, I. V. Tokatly, and A. Rubio, Quantum-electrodynamical density-functional theory: Bridging quantum optics and electronic-structure theory, *Phys. Rev. A* **90**, 012508 (2014).
- [21] M. Farzanehpour and I. V. Tokatly, Quantum electrodynamical time-dependent density-functional theory for many-electron systems on a lattice, *Phys. Rev. B* **90**, 195149 (2014).
- [22] C. Pellegrini, J. Flick, I. V. Tokatly, H. Appel, and A. Rubio, Optimized effective potential for quantum electrodynamical time-dependent density functional theory, *Phys. Rev. Lett.* **115**, 093001 (2015).
- [23] J. Flick, M. Ruggenthaler, H. Appel, and A. Rubio, Kohn-Sham approach to quantum electrodynamical density-functional theory: Exact time-dependent effective potentials in real space, *Proc. Natl. Acad. Sci. USA* **112**, 15285 (2015).
- [24] M. Ruggenthaler, Ground-state quantum-electrodynamical density-functional theory, [arXiv:1509.01417](https://arxiv.org/abs/1509.01417).
- [25] T. Jaako, Z.-L. Xiang, J. J. Garcia-Ripoll, and P. Rabl, Ultrastrong-coupling phenomena beyond the Dicke model, *Phys. Rev. A* **94**, 033850 (2016).
- [26] P. Pilar, D. De Bernardis, and P. Rabl, Thermodynamics of ultrastrongly coupled light-matter systems, *Quantum* **4**, 335 (2020).
- [27] D. De Bernardis, T. Jaako, and P. Rabl, Cavity quantum electrodynamics in the nonperturbative regime, *Phys. Rev. A* **97**, 043820 (2018).
- [28] M. Schuler, D. De Bernardis, A. M. Läuchli, and P. Rabl, The vacua of dipolar cavity quantum electrodynamics, *SciPost Phys.* **9**, 066 (2020).
- [29] L. Lamata, Digital-analog quantum simulation of generalized Dicke models with superconducting circuits, *Sci. Rep.* **7**, 43768 (2017).
- [30] D. S. Shapiro, W. V. Pogosov, and Y. E. Lozovik, Universal fluctuations and squeezing in a generalized Dicke model near the superradiant phase transition, *Phys. Rev. A* **102**, 023703 (2020).
- [31] F. M. Gambetta, I. Lesanovsky, and W. Li, Exploring nonequilibrium phases of the generalized dicke model with a trapped

- Rydberg-ion quantum simulator, *Phys. Rev. A* **100**, 022513 (2019).
- [32] K. Akbari, W. Salmon, F. Nori, and S. Hughes, Generalized Dicke model and gauge-invariant master equations for two atoms in ultrastrongly-coupled cavity quantum electrodynamics, *Phys. Rev. Res.* **5**, 033002 (2023).
- [33] D. De Bernardis, P. Pilar, T. Jaako, S. De Liberato, and P. Rabl, Breakdown of gauge invariance in ultrastrong-coupling cavity QED, *Phys. Rev. A* **98**, 053819 (2018).
- [34] G. M. Andolina, F. M. D. Pellegrino, V. Giovannetti, A. H. MacDonald, and M. Polini, Cavity quantum electrodynamics of strongly correlated electron systems: A no-go theorem for photon condensation, *Phys. Rev. B* **100**, 121109(R) (2019).
- [35] G. M. Andolina, F. M. D. Pellegrino, V. Giovannetti, A. H. MacDonald, and M. Polini, Theory of photon condensation in a spatially varying electromagnetic field, *Phys. Rev. B* **102**, 125137 (2020).
- [36] See Supplemental Material at <http://link.aps.org/supplemental/10.1103/PhysRevA.108.L051701> for Polarization dependencies on external potential for different combinations of  $N_1, N_2$ , calculation of diagrams contributing to the ground state energy.
- [37] J. Flick, H. Appel, M. Ruggenthaler, and A. Rubio, Cavity born Oppenheimer approximation for correlated electron nuclear-photon systems, *J. Chem. Theory Comput.* **13**, 1616 (2017).
- [38] Y.-Y. Liu, K. D. Petersson, J. Stehlik, J. M. Taylor, and J. R. Petta, Photon emission from a cavity-coupled double quantum dot, *Phys. Rev. Lett.* **113**, 036801 (2014).
- [39] G.-W. Deng, D. Wei, S.-X. Li, J. R. Johansson, W.-C. Kong, H.-O. Li, G. Cao, M. Xiao, G.-C. Guo, F. Nori *et al.*, Coupling two distant double quantum dots with a microwave resonator, *Nano Lett.* **15**, 6620 (2015).
- [40] Y.-Y. Liu, J. Stehlik, C. Eichler, M. J. Gullans, J. M. Taylor, and J. R. Petta, Semiconductor double quantum dot micromaser, *Science* **347**, 285 (2015).
- [41] M. Cirio, S. De Liberato, N. Lambert, and F. Nori, Ground state electroluminescence, *Phys. Rev. Lett.* **116**, 113601 (2016).